Letters

Dual-Frequency Ultra-Wide-Load Resonant Inverter for Electrosurgical Generator System

Yifan Jiang, Xinlin Wang, *Student Member, IEEE*, Jun Yang, Junrui Liang, *Senior Member, IEEE*, Haoyu Wang, *Member, IEEE*, and Minfan Fu, *Senior Member, IEEE*

***Abstract*—This letter presents a dual-frequency electrosurgical generator (ESG) based on a Class EF inverter, designed to accommodate ultra-wide impedance variations encountered during surgical procedures. The inherent load-insensitive characteristics of the Class EF inverter at a single frequency are further enhanced through the adoption of a dual-frequency operation strategy. To explore the design potential, inequality constraints and an impedance-based analysis method are employed. High operational efficiency is established as the primary design goal, and a simple dual-frequency and current control scheme is implemented to maintain stable output power. In the experimental validation, a 3/4-MHz ESG system is developed, achieving an efficiency above 63% and delivering 20 W of output power across a wide load range of 50–1500 Ω.**

***Index Terms*—Dual-frequency design, electrosurgical generator (ESG), inequality constraints, ultra-wide load variation.**

I. Introduction

Electrosurgical generators (ESG) have been widely used in surgical operations, such as laparoscopy, arthroscopy, and tumor ablation. The traditional electrocautery utilizes the electrical current to heat the metallic probe and apply it to body tissue. Unlike electrocautery generators, ESG achieves the surgical effect (such as cutting and coagulation) through high-frequency electrical current [1], [2], [3]. A low-frequency alternating current would cause neuromuscular excitation, which would lead to pain, muscle contraction, and even cardiac arrhythmia. As the frequency increases, such neuromuscular stimulation would be negligible, and it would also help the energy transfer inside the tissue cells. The increasing switching frequency of the ESG system enables fast cutting and deep coagulation and would reduce intraoperative bleeding during the surgery.

During surgical procedures, the equivalent load of body tissue varies significantly due to the constantly changing morphology at the surgical site. This variation includes both resistive and reactive components, posing challenges for stable and efficient power delivery. Conventional solutions, such as full-bridge converters at kHz frequencies [4], [5] and impedance matching networks (IMNs) [6], [7], introduce additional complexity or are limited in frequency scalability. Moreover, fluctuations in delivered energy can lead to inconsistent cutting depth or coagulation, increasing the risk of thermal injury to surrounding nerves and organs. Therefore, achieving a load-insensitive and power-stable ESG system, especially at high frequencies, is critical for surgical safety and clinical effectiveness.

To meet this demand, this letter proposes a dual-frequency ESG system based on a Class EF inverter, aiming to enhance load adaptability while maintaining stable output power without relying on extra IMNs. To address these challenges, a dual-frequency design methodology is proposed to further extend the load-insensitive operating range of the inverter with different frequencies optimized for different segments of the load range. The integration of an inequality-constraint-based design approach with an impedance model facilitates efficient exploration of the design space and leverages the inverter's high degree of freedom. A simple current control strategy is adopted to ensure stable output power without the need for additional IMNs. Experimental results demonstrate that the proposed ESG system achieves high efficiency and stable output power across a broad range of load conditions.

II. Ultra-Wide Load Insensitive Design

A. System Configuration

The circuit model of the proposed ESG system is illustrated in Fig. 1. Due to the high switching frequency, parasitic components of the electrosurgical instrument need to be considered. It is modeled as a T-network, and the corresponding component

Received 25 June 2025; revised 25 August 2025 and 30 September 2025; accepted 20 October 2025. Date of publication 3 November 2025; date of current version 23 December 2025. This work was supported in part by the National Natural Science Foundation of China under Grant 52477013 and in part by the Lingang Laboratory under Grant LG-GG-202402-06-10. *(Yifan Jiang and Xinlin Wang are co-first authors.) (Corresponding author: Minfan Fu.)*

Yifan Jiang is with Electric Power Research Institute, State Grid Liaoning Electric Power Company, Ltd., Shenyang 110006, China, and also with the School of Information Science and Technology, ShanghaiTech University, Shanghai 201210, China.

Xinlin Wang and Jun Yang are with the School of Information Science and Technology, ShanghaiTech University, Shanghai 201210, China.

Junrui Liang, Haoyu Wang, and Minfan Fu are with the School of Information Science and Technology, ShanghaiTech University, Shanghai 201210, China, and also with the Shanghai Engineering Research Center of Energy Efficient and Custom AI IC, Shanghai 201210, China (e-mail: fumf@shanghaitech.edu.cn).

Color versions of one or more figures in this article are available at https://doi.org/10.1109/TPEL.2025.3625568.

Digital Object Identifier 10.1109/TPEL.2025.3625568

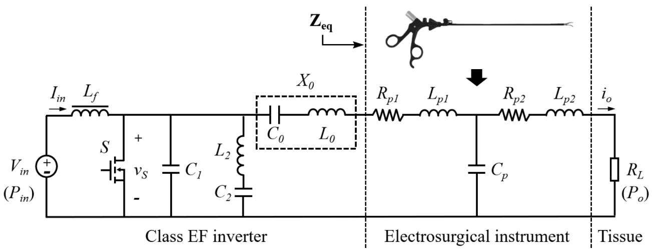

Fig. 1. Equivalent circuit model of the proposed ESG.

TABLE I
ELECTROSURGICAL INSTRUMENT PARAMETERS

Symbol	R_{p1}	R_{p2}	L_{p1}	L_{p2}	C_p
Value	5.9	0.6	1.15	0.56	0.202

Inductance unit: μH; Capacitance unit: nF; Resistance unit: Ω.

values are measured and given in Table I [6]. Note that the body tissue is modeled as a resistor R_L, which would vary within a wide range during the surgical process. During operation, the variable load resistance R_L is transformed into a corresponding load impedance $\mathbf{Z_{eq}}$ via the T-network of the surgical instrument. Consequently, the Class EF inverter must directly accommodate the varying impedance $\mathbf{Z_{eq}}$. The inverter consists of a single switch S operating at a switching frequency f_s, with a duty cycle denoted by D. An inductor L_f functions as an RF choke, while the shunt capacitor C_1 compensates for the switch's junction capacitance. The components L_2 and C_2 are designed to resonate at the frequency f_2, which means

$$f_2 = 1/\left(2\pi\sqrt{L_2 C_2}\right). \tag{1}$$

L_0 and C_0 resonate at f_s, with an additional reactance X_0

$$X_0 = \omega_s L_0 - 1/\left(\omega_s C_0\right). \tag{2}$$

B. Dual-Frequency Design

Single-switch resonant inverters are widely employed for high-frequency excitation due to their simplicity and their potential for load-insensitive operation [8], [9]. Nevertheless, many existing designs operate at a fixed switching frequency, typically constrained by specific application requirements. In the application addressed in this study, the primary objective is to deliver high-frequency current to a surgical site, where the operating frequency is permitted to vary within a range of several megahertz. By exploiting the inherent load-insensitive characteristics of single-switch resonant inverters, this letter introduces a dual-frequency operation strategy along with its corresponding design methodology, aiming to enhance the inverter's adaptability to varying loads.

As illustrated in Fig. 1, the design involves five parameters: C_0, C_1, C_2, L_0, and L_2. Since precise tuning of inductors is not feasible, the values of L_0 and L_2 are fixed. Based on (1) and (2), the inverter design under a specified duty cycle D includes three degrees of freedom: f_2, C_1, and C_0. The inverter efficiency is calculated using

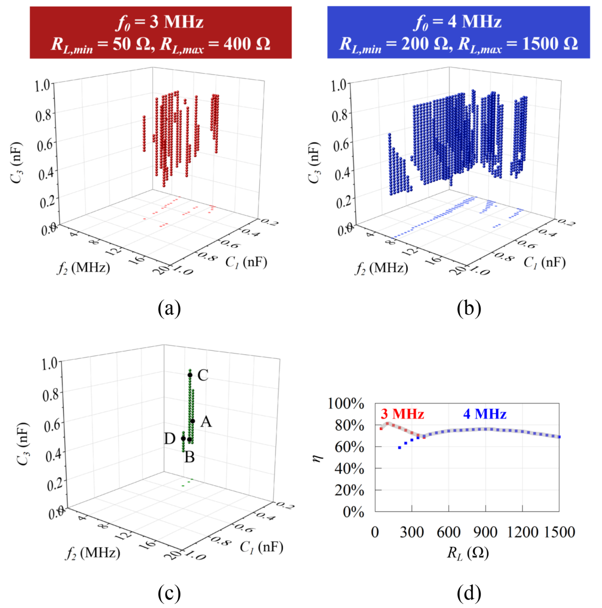

Fig. 2. Dual-frequency inverter. (a) f_0=3 MHz. (b) f_0=4 MHz. (c) Parameter selection space. (d) η-R_L for Case D.

$$\eta = \frac{P_o}{P_{\text{in}}} = \frac{I_{o,\text{rms}}^2 R_L}{V_{\text{in}} I_{\text{in}}} \tag{3}$$

where P_o denotes the output power delivered to the tissue, P_{in} is the input power of the inverter, $I_{o,\text{rms}}$ is the output rms current, and V_{in} and I_{in} are the input voltage and current, respectively. To ensure high efficiency of the ESG system across varying loads, a traditional system must satisfy the following constraints:

$$\begin{cases} R_{L,\min} < R_L < R_{L,\max} \\ \eta > \eta_{\min} \\ f_s = f_0. \end{cases} \tag{4}$$

This means that the inverter efficiency η must exceed $\eta_{\min}$ for all load resistances R_L within the range $[R_{L,\min}, R_{L,\max}]$, with a fixed switching frequency $f_s = f_0$.

A target system is conducted using the following parameters: $D = 0.5$, $V_{\text{in}} = 40$ V, $L_f = 47\,\mu$H, $L_0 = 10\,\mu$H, and $L_2 = 1\,\mu$H. The design goal is to achieve a minimum efficiency of $\eta_{\min} = 55\%$, with R_L ranging from 50 to 1500 Ω. To handle the ultra-wide load variation observed during surgical operation, the switching frequency f_s is considered as a design variable. In addition, f_2, C_1, and C_0 are selected as the remaining three design variables. Utilizing the extended impedance method [10], the system state equations can be solved for specified parameter values, thereby enabling an efficient sweep of the 4-D design space.

The whole design process is illustrated in Fig. 2. Initially, a 3-MHz inverter is evaluated under the following design constraints: $R_{L,\min} = 50\,\Omega$, $R_{L,\max} = 400\,\Omega$, $\eta_{\min} = 55\%$, and $f_0 = 3$ MHz. Parameter sweeping via the extended impedance method rapidly identifies feasible design candidates, as shown

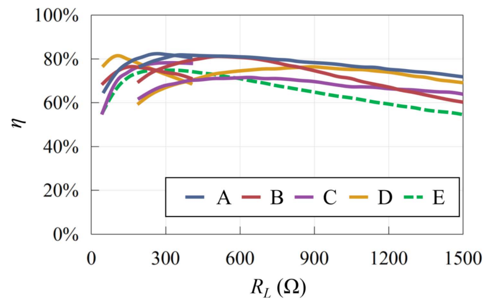

Fig. 3. Benefits of dual-frequency system efficiency.

in Fig. 2(a). Similarly, a 4-MHz inverter is analyzed with updated constraints: $R_{L,\min} = 200\,\Omega$, $R_{L,\max} = 1500\,\Omega$, $\eta_{\min} = 55\%$, and $f_0 = 4$ MHz, which corresponds to a typical operating frequency used in commercial ESG systems [11]. Note that f_0=3 MHz and f_0=4 MHz only showcase the proposed dual-frequency ESG system. The corresponding design points are illustrated in Fig. 2(b). The combined solution space is shown in Fig. 2(c), indicating that all identified points satisfy the constraints of Figs. 2(a) and (b).

Four representative cases (A–D) are selected for further analysis. As an example, Fig. 2(d) demonstrates the efficiency performance of Case D, highlighting that the proposed dual-frequency design can maintain high efficiency through frequency switching at a boundary load condition. Similarly, the efficiency of four cases is compared in Fig. 3 (indicated as solid lines). By frequency selection, all these systems can maintain high efficiency across the load range. Favorable efficiency performance would be ensured based on practical demands.

Following the same design methodology, a system can also be configured to cover a wide load range using a single operating frequency. As an example, Case E (indicated as a dotted line in Fig. 3) is designed with $R_{L,\min} = 50\,\Omega$, $R_{L,\max} = 1500\,\Omega$, $\eta_{\min} = 55\%$, and $f_0 = 3\,$MHz. However, the resulting efficiency is not attractive under such an ultra-wide load condition.

C. Maintaining Stable Output Power

The design considerations in the previous section ensure dual-frequency, high-efficiency operation over a wide load range. In this section, the focus is further extended toward exploring design strategies for control simplification. Maintaining a stable output power is sufficient to achieve the desired thermal effect during surgery. Furthermore, implementing a closed-loop power controller based on output power detection is also unrealistic in heat-generation application. To address this, a buck converter is employed as the prestage of the Class EF inverter, as shown in Fig. 4. The proposed work simplifies the buck converter control by exploiting the inherent characteristics of the dual-frequency inverter, enabling the system to regulate a readily measurable state variable (i.e., the input of the inverter) to maintain stable output power over an ultra-wide load range.

Using the impedance-based circuit model, the input current and voltage of the inverter (i.e., I_{in} and V_{in}) required to achieve a

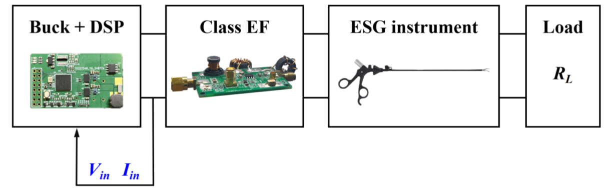

Fig. 4. Maintain stable output power based on a buck converter (final real system).

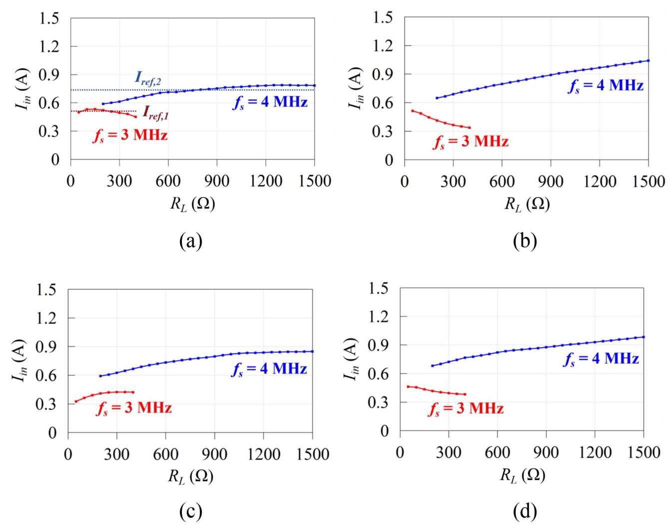

Fig. 5. I_{in}-R_L when P_{ref}=20 W. (a) Case A. (b) Case B. (c) Case C. (d) Case D.

stable output power $P_o = P_{\text{ref}}$ can be calculated across varying load resistances R_L. The resulting I_{in}–R_L curves for $P_{\text{ref}} = 20$ W are shown in Fig. 5 for the four selected cases. In each plot, the dual switching frequencies are indicated by red and blue lines, respectively. Among which, Case A exhibits the smallest input current variation within each frequency mode, indicating that the buck converter can be operated under current control to drive the Case A-based inverter. Notably, two reference currents are required, corresponding to the two switching frequencies [refer to I_{ref1} and I_{ref2} in Fig. 5(a)].

Based on the selected I_{ref} in Fig. 5(a), the corresponding output power is illustrated in Fig. 6(a). The results indicate that, under the control strategy, the power remains stable at approximately 20 W. The target output power P_{ref} is the first input to the system. An overlapping region appears around 300 Ω. To distinguish between the two operating modes, the input voltage V_{in} is monitored for mode selection, as depicted in Fig. 6(b). For example, $V_{\max,1}$ and $V_{\max,2}$ represent the voltage thresholds for transitioning between the 3-MHz and 4-MHz modes, respectively, while $I_{\text{ref},1}$ and $I_{\text{ref},2}$ correspond to the respective reference currents. When operating at $f_s = 3\,$MHz (or 4 MHz), if V_{in} exceeds $V_{\max,1}$ (or $V_{\max,2}$), the system switches frequency and updates I_{ref} accordingly. A hysteresis region is introduced as the overlap between the two frequency bands to prevent frequent switching. Finally, a low-bandwidth current control loop is implemented for the buck converter in Fig. 6(c). The control loop monitors V_{in} for mode selection and subsequently

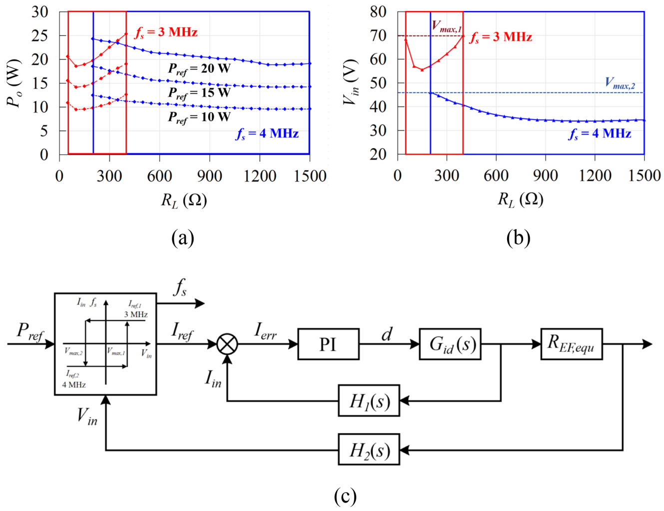

Fig. 6. Output power control. (a) Inverter output power P_o. (b) Inverter input voltage V_{in} when P_{ref}=20 W. (c) Control block diagram.

TABLE II
SYSTEM PARAMETERS

Component	Value/Parameter	Component	Value/Parameter
f_s	3 / 4	D	0.5
Switch S	GS66508T	Driver	ISL55110IVZ
L_f	47; Coilcraft	C_0	0.45; TDK C0G
L_0	9.95; Hand-wound	C_1	0.10; TDK C0G
L_2	0.99; Hand-wound	C_2	0.81; TDK C0G

Frequency unit: MHz; Inductance unit: μH; Capacitance unit: nF.

generates I_{ref} for the current controller, which is sufficient to satisfy the heat-generation requirements. In practice, when the target output power needs to be adjusted, it can be manually tuned through an analog input P_{ref}. Output power when P_{ref}=15 W and P_{ref}=10 W are given as examples and illustrated in Fig. 6(a) to verify the feasibility of various power levels.

III. Experimental Verification

A prototype of the proposed ESG system is implemented in Fig. 4. The equivalent load of the body tissue is manually tuned by a real resistor, which varies from 50 to 1500 Ω. GS66508T from GaN Systems is selected as the switch. The whole system parameters are given in Table II.

The measured efficiency and inverter input voltage when P_{ref}=20 W are illustrated in Fig. 7(a). Under the two frequency modes, the inverter maintains an efficiency above 63%, reaching a peak of 84%. The output power delivered to the load remains around the corresponding P_{ref}, effectively maintaining stable output power [as is shown in Fig. 7(b)]. Various target output power that are needed in the surgery would be realized by adjusting P_{ref}. The measured output power as P_{ref}=15 and 10 W are presented.

Fig. 8 shows the experimental waveforms of the proposed dual-frequency ESG system. Six representative load conditions were tested, demonstrating stable output power operation across a wide range. Notably, the transistor waveforms (v_s) differ from

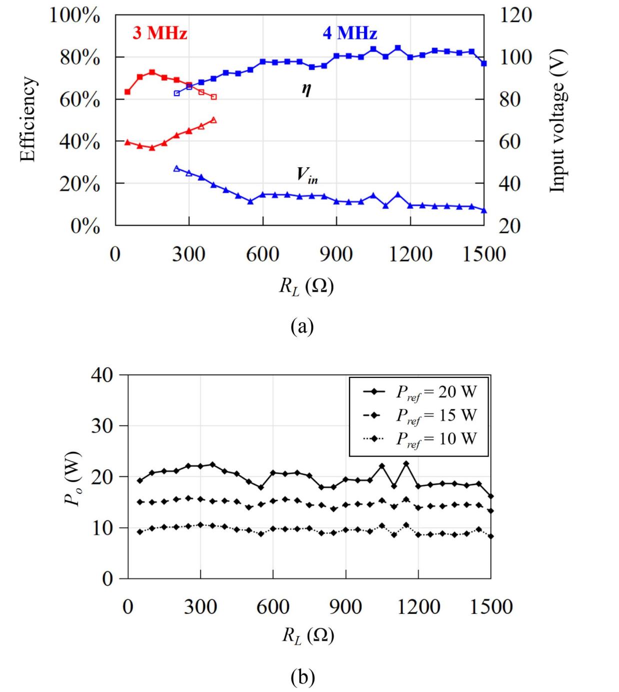

Fig. 7. Experimental results. (a) Measured efficiency and inverter input voltage when P_{ref}=20 W. (b) Measured output power.

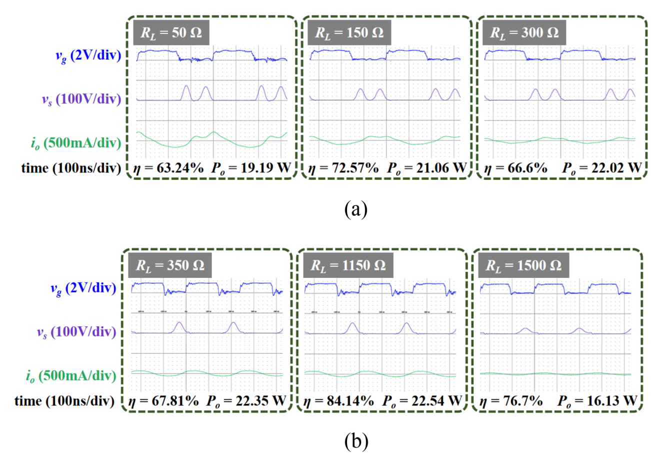

Fig. 8. Experimental waveform. (a) f_s=3 MHz. (b) f_s=4 MHz.

those observed in conventional Class EF inverters operating under fixed load and fixed frequency conditions. The proposed design enables zero-voltage switching operation over a wide operating range. Fig. 9 illustrates the transition process between the two frequency modes. Voltage and current waveforms during mode switching are presented.

Table III compares the performance of various ESG applications. Note that IMN represents the impedance matching network in the system. By adopting the proposed dual-frequency design, the load range has been expanded from eight times (when f_s=3 MHz) and six times (when f_s=4 MHz) to 30 times. The proposed dual-frequency resonant inverter illustrates a balance point between efficiency and load adaptability. It would ensure

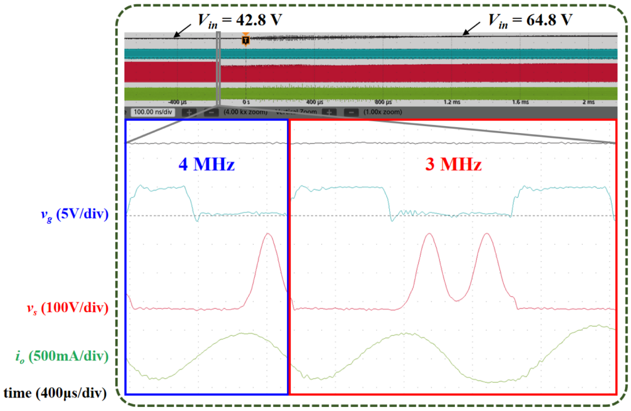

Fig. 9. Transient waveforms during mode selection.

TABLE III
COMPARISON OF VARIOUS ESGS

Ref	Inverter	f_s (MHz)	R_L (Ω)	$\frac{R_{L,\max}}{R_{L,\min}}$	η	P_o (W)	IMN
[6]	Full-bridge	3.5/4	[5,800]	160	[60.2%,66.7%]	60/80/100	Yes
[7]	Full-bridge	4	[10,200]	20	[60%,88%]	20/50/70	Yes
[12]	Four-phase buck	2	[300,4000]	13.3	-	10/50	No
[11]	-	4	-	-	-	50	-
This	Class EF	3/4	[50,1500]	30	[63%,84%]	20	No

the high-efficiency operation under ultra-wide load without an extra IMN.

IV. CONCLUSION

This letter proposes a dual-frequency ESG system powered by a load-insensitive Class EF inverter. Inequality constraints are incorporated into the design process to enhance design flexibility. To accommodate a wide range of load variations, a dual-frequency approach is adopted, and a simple current control scheme is employed to fulfill the stable output power requirement. The ESG system achieves high-efficiency performance (i.e., 63%–84%) while maintaining stable output power through a straightforward control strategy.

REFERENCES

[1] A. Taheri, P. Mansoori, L. F. Sandoval, S. R. Feldman, and D. P. P. M. Williford, "Electrosurgery: Part I. basics and principles," *J. Am Acad. Dermatol.*, vol. 70, no. 4, pp. 591.e1–591.e14, 2014.

[2] C. Bao and S. K. Mazumder, "Reduced collateral tissue damage using thermal-feedback-based power adaptation of an electrosurgery inverter," *IEEE Trans. Power Electron.*, vol. 37, no. 10, pp. 11540–11545, Oct. 2022.

[3] M. Mohsin Rafiq, N. Ullah, L. Prokop, S. Misak, V. Blazek, and M. Ishfaq, "Artificial intelligence-enhanced peak current mode control for enhanced power regulation in high power high frequency electrosurgical generators," *IEEE Access*, vol. 12, pp. 149045–149060, 2024.

[4] D. A. Friedrichs, R. W. Erickson, and J. Gilbert, "A new dual current-mode controller improves power regulation in electrosurgical generators," *IEEE Trans. Biomed. Circuits Syst.*, vol. 6, no. 1, pp. 39–44, Feb. 2012.

[5] C. Bao and S. K. Mazumder, "Multiresonant-frequency filter for an electrosurgery inverter," *IEEE Trans. Power Electron.*, vol. 37, no. 6, pp. 6242–6246, Jun. 2022.

[6] B. Yoon et al., "4 MHz electrosurgical generator system for wide load impedance range with SiC-based full-bridge inverter," *IEEE Trans. Ind. Electron.*, vol. 71, no. 1, pp. 338–347, Jan. 2024.

[7] S. Hwang et al., "GaN-Based 4-MHz full-bridge electrosurgical generator using zero-voltage switching over wide load impedance range," *IEEE Trans. Biomed. Circuits Syst.*, vol. 17, no. 5, pp. 1125–1134, Oct. 2023.

[8] Y. Cheng, Y. Guan, T. Yao, Y. Wang, W. Wang, and D. Xu, "Topology construction strategy of load-independent single-switch resonant inverter," *IEEE Trans. Ind. Electron.*, vol. 71, no. 9, pp. 10580–10590, Sep. 2024.

[9] S. Aldhaher, D. C. Yates, and P. D. Mitcheson, "Load-independent class E/EF inverters and rectifiers for MHz-Switching applications," *IEEE Trans. Power Electron.*, vol. 33, no. 10, pp. 8270–8287, Oct. 2018.

[10] Y. Jiang, H. Li, Y. Liu, J. Liang, H. Wang, and M. Fu, "Multiconstraint design of single-switch resonant converters based on extended impedance method," *IEEE J. Emerg. Sel. Top. Power Electron.*, vol. 11, no. 2, pp. 1901–1912, Apr. 2023.

[11] *Radiofrequency Energy Sources & Accessory Products*, Ellman, Catalogs, 2017.

[12] S. Jensen and D. Maksimovic, "Fast tracking electrosurgical generator using two-rail multiphase buck converter with GaN switches," *IEEE Trans. Power Electron.*, vol. 32, no. 1, pp. 634–641, Jan. 2017.